

M. Stenroos and J. Haueisen. 2008. Boundary element computations in the forward and inverse problems of electrocardiography: comparison of collocation and Galerkin weightings. IEEE Transactions on Biomedical Engineering, volume 55, number 9, pages 2124-2133.

© 2008 IEEE

Reprinted with permission.

This material is posted here with permission of the IEEE. Such permission of the IEEE does not in any way imply IEEE endorsement of any of Helsinki University of Technology's products or services. Internal or personal use of this material is permitted. However, permission to reprint/republish this material for advertising or promotional purposes or for creating new collective works for resale or redistribution must be obtained from the IEEE by writing to pubs-permissions@ieee.org.

By choosing to view this document, you agree to all provisions of the copyright laws protecting it.

Boundary Element Computations in the Forward and Inverse Problems of Electrocardiography: Comparison of Collocation and Galerkin Weightings

Matti Stenroos* and Jens Haueisen

Abstract—In electrocardiographic imaging (ECGI), epicardial potentials are reconstructed computationally from electrocardiographic measurements. The reconstruction is typically done with help of the boundary element method (BEM), using the point collocation weighting and constant or linear basis functions. In this work, we evaluated the performance of constant and linear point collocation and Galerkin BEMs in the epicardial potential problem.

The integral equations and discretizations were formulated in terms of the single- and double-layer operators. All inner element integrals were calculated analytically. The computational methods were validated against analytical solutions in a simplified geometry. On the basis of the validation, no method was optimal in all testing scenarios.

In the forward computation of the epicardial potential, the linear Galerkin (LG) method produced the smallest errors. The LG method also produced the smallest discretization error on the epicardial surface. In the inverse computation of epicardial potential, the electrode-specific transfer matrix performed better than the full transfer matrix. The Tikhonov 2 regularization outperformed the Tikhonov 0. In the optimal modeling conditions, the best BEM technique depended on electrode positions and chosen error measure. When large modeling errors such as omission of the lungs were present, the choice of the basis and weighting functions was not significant.

Index Terms—Boundary element methods, Electrocardiography, Galerkin method, Forward problem, Inverse problem

I. INTRODUCTION

Electrocardiographic imaging (ECGI) [1]–[3] is a promising non-invasive method for the characterization of cardiac electrical events. In ECGI, epicardial potentials are reconstructed computationally from electrocardiographic measurements performed on the body surface. The field computations in ECGI and other cardiac inverse modeling scenarios are commonly done with help of the boundary element method (BEM) [4].

In the BEM, the boundary potentials are discretized into linear combinations of basis functions, and the weighted

residual of the discretized solution is minimized [4]. There are two commonly used weighting methods: the point collocation and the Galerkin method. In the point collocation method, the residual is minimized in a set of discrete points on the boundary surfaces. In the Galerkin method, the integral of the residual over the boundary surfaces is minimized. ECGI and other epicardial potential modeling studies utilizing the BEM have so far been done with point collocation weighting and mostly with constant [5]–[7] and linear basis functions [8], [9].

In this work, we present the application of the constant and linear Galerkin methods to the forward and inverse problems of electrocardiography in terms of epicardial potential. We compare these methods to the constant and linear point collocation methods. Further, we assess the influence of modeling errors on the simulation results obtained with all four methods.

While the epicardial potential problem is formulated directly in terms of potential outside the source region, other approaches to the forward and inverse problems of electrocardiography utilize source models, e.g., transmbrane potential distributions (TMP) [10]–[13] or uniform double layers (UDL) [14]. The UDL model aims at directly solving for the activation wavefronts, and TMP models are used in activation time imaging (ATI), too [11]–[13]. In analytical validation studies on forward computation with the TMP model, the Galerkin weighting has performed better than the collocation weighting [11], [13]. Because of the different mathematical approaches, these results can not be generalized to the epicardial potential problem: In the epicardial potential problem, both single- and double-layer integral operations need to be discretized, while in source modeling problems, double-layer integral operations and the infinite medium potential due to the sources are used. In ATI, a priori information on cardiac activation is also used in a way advantageous to the Galerkin method [11]. Advantages and limitations of different approaches are discussed in [15].

In addition to the BEM, the epicardial and transmbrane potential problems have been solved with the finite element method (FEM) [13], [16], [17]. The main advantage of the FEM is the possibility to model anisotropic structures. If isotropic, piece-wise homogeneous models are used, the FEM does not seem to offer benefits [13]. It is also possible to use the BEM elsewhere, but FEM in anisotropic compartments [18].

For neuroscientific applications, the point collocation and Galerkin methods have been evaluated in simplified and brain-

Manuscript received October 7, 2007; revised January 23 and February 25, 2008. This work was funded by the Academy of Finland, German Academic Exchange Service, EU project NMP4-CT-2005-017002, and Foundation of Technology in Finland. *Asterisk indicates corresponding author.*

M. Stenroos is with the Helsinki University of Technology, Department of Biomedical Engineering and Computational Science, P.O. Box 2200, FI-02015 TKK, Finland.

J. Haueisen is with Technische Universität Ilmenau, Institute for Biomedical Engineering and Informatics, P.O. Box 100565, D-98684 Ilmenau, Germany, and Biomagnetic Center Jena, Erlanger Allee 101, D-07747 Jena, Germany.

Copyright © 2008 IEEE. Personal use of this material is permitted. However, permission to use this material for any other purposes must be obtained from the IEEE by sending an email to pubs-permissions@ieee.org.

shaped volume conductors with a dipolar source model. The results of Tissari and Rahola [19] and Mosher et al. [20] are in favor of the Galerkin method.

It has been suggested [21] that a homogeneous volume conductor model is adequate for the epicardial potential problem. After that study, an inhomogeneous BEM model has, to our knowledge, not been used in the epicardial potential problem. Therefore, the homogeneous model is used as starting point in this study, too. Also error measures and regularization methods are chosen according to common practice in epicardial potential computations.

II. METHODS

A. Integral Equations for the Electric Potential in a Volume Conductor

In a volume conductor under quasi-static conditions [22], the electric potential ϕ generated by slowly varying primary currents \vec{J}_p obeys the Poisson equation

$$\nabla \cdot (\sigma \nabla \phi) = \nabla \cdot \vec{J}_p, \quad (1)$$

where σ is the electric conductivity. In order to do boundary element modeling, the Poisson equation is converted to surface integral form with the Green theorem. To keep the notation compact, we present the integral equations in terms of single- and double-layer operators G and D :

$$G^{kl}[f](\vec{r}) = \frac{1}{4\pi} \int_{S^l} \frac{f(\vec{r}')}{|\vec{r} - \vec{r}'|} dS', \quad \vec{r} \in S^k \quad (2)$$

$$D^{kl}[g](\vec{r}) = \frac{1}{4\pi} \int_{S^l} g(\vec{r}') \frac{(\vec{r} - \vec{r}')}{|\vec{r} - \vec{r}'|^3} \cdot d\vec{S}', \quad \vec{r} \in S^k, \quad (3)$$

where \vec{r} and \vec{r}' are position vectors in field and source coordinates, and superscripts k and l label the field and source surfaces, respectively. Surfaces are labeled with S , and f and g refer to functions, which the operators act on. In all following equations, the first superscript labels the field surface and the second superscript the source surface. If there is only one superscript, it labels the source surface.

In case of a finite homogeneous volume conductor with known primary current distribution inside the conductor, the integral equation for the surface potential [23], [24] reads

$$\phi^B = 2\phi_\infty^B - 2D^{BB}[\phi^B] \quad (4)$$

with

$$\phi_\infty^B(\vec{r}) = \frac{1}{4\pi\sigma} \int_{V_s} \frac{\vec{J}_p \cdot (\vec{r} - \vec{r}')}{|\vec{r} - \vec{r}'|^3} dV', \quad (5)$$

where superscript ‘‘B’’ labels the boundary surface of the model — in this work the body surface — and V_s the volume containing all the sources, σ is the conductivity inside the thorax, and ϕ_∞ is the potential generated by \vec{J}_p in an infinite, homogeneous volume conductor. When the surface potential ϕ^B is known, the potential inside the volume conductor can be calculated with [23]

$$\phi(\vec{r}) = \phi_\infty(\vec{r}) - D^B[\phi^B](\vec{r}), \quad (6)$$

where D^B is the double layer operator of (3) with free \vec{r} .

In order to use (4), the source distribution needs to be modelled. This equation with varying forms of ϕ_∞^B is the

starting point in, e.g., TMP and UDL modeling. The epicardial potential problem is formulated outside the source region. Thus it can be solved directly in terms of potential. Consequently, no source models are needed. In a homogeneous thoracic volume conductor model, this potential problem leads to an equation pair [5], [6]. Utilizing the operator notation, we get

$$\frac{1}{2}\phi^H = -D^{HB}[\phi^B] + D^{HH}[\phi^H] - G^{HH}[\Gamma^H] \quad (7)$$

$$\frac{1}{2}\phi^B = -D^{BB}[\phi^B] + D^{BH}[\phi^H] - G^{BH}[\Gamma^H], \quad (8)$$

where superscripts ‘‘B’’ and ‘‘H’’ label the body surface and the outer surface of the heart muscle (epicardium), and $\Gamma^H = \partial\phi^H/\partial n$ is the normal component of the potential gradient on the epicardial surface.

B. Boundary Element Discretization

To solve the potential from the surface integral equations, the surface potentials are discretized with the boundary element method [4], [25]. The discretization procedure consists of three phases: tessellation of the boundary surfaces, approximation of the boundary potentials with a linear combination of polynomial basis functions ψ , and minimization of the error of the approximated solution with respect to some weight functions w . In this work, the surfaces are tessellated into flat triangles, and the basis functions are defined according to either the nodes or triangles of the mesh.

In case of constant basis functions, each basis function has the value 1 in one triangle and value 0 elsewhere. The number of basis functions thus corresponds to the number of triangles in the surface model. Linear basis functions are, on the contrary, defined according to the nodes of the mesh: A linear basis function is defined in the neighborhood of a node. It has the value 1 in one node, and the value falls linearly to zero towards the neighboring nodes.

A general boundary potential can not be accurately represented with a limited set of pre-defined basis functions. The error resulting from the application of basis functions is minimized with respect to a set of linearly independent weight functions. The number of weight functions is chosen the same as the number of basis functions N . Application of basis and weight functions leads thus to a system of N linear equations with N unknowns.

The most simple weighting method is the point collocation method, in which the residual is minimized in a discrete set of points, defined with the Dirac δ functions. This point set consists of the centroids of the mesh triangles in case of constant basis functions, and of the mesh nodes in case of linear basis functions. Another option is to minimize the residual over the whole surfaces instead of discrete points. This is the aim of the Galerkin method, in which the weight functions are chosen identical with the basis functions. The points, in which the Galerkin solution is calculated, are the same as in the collocation solution. These definition points of the Galerkin weight functions are in this work, for clarity, also called the collocation points. The Galerkin solution is, however, not optimized for accuracy in these points.

C. Discretization of the Integral Equations

Discretization of (4), (7), and (8) leads to

$$\mathbf{A}^B \Phi^B = 2\mathbf{B} - 2\mathbf{D}^{BB} \Phi^B \quad (9)$$

$$\frac{1}{2} \mathbf{A}^H \Phi^H = -\mathbf{D}^{HB} \Phi^B + \mathbf{D}^{HH} \Phi^H - \mathbf{G}^{HH} \Gamma^H \quad (10)$$

$$\frac{1}{2} \mathbf{A}^B \Phi^B = -\mathbf{D}^{BB} \Phi^B + \mathbf{D}^{BH} \Phi^H - \mathbf{G}^{BH} \Gamma^H, \quad (11)$$

where Φ^H , Φ^B , and Γ contain values of ϕ^H , ϕ^B , and Γ^H in the collocation points, and \mathbf{A} , \mathbf{B} , \mathbf{D} , and \mathbf{G} are matrices with elements

$$\mathbf{A}_{ij}^k = \int_{S^k} w_i^k \psi_j^k dS \quad (12)$$

$$\mathbf{B}_i^k = \int_{S^k} w_i^k \phi_\infty dS \quad (13)$$

$$\mathbf{D}_{ij}^{kl} = \int_{S^k} w_i^k D^{kl}[\psi_j^l] dS \quad (14)$$

$$\mathbf{G}_{ij}^{kl} = \int_{S^k} w_i^k G^{kl}[\psi_j^l] dS, \quad (15)$$

in which w_i^k is the i th weight function on surface k , and ψ_j^l is the j th basis function on surface l .

1) *Point Collocation*: In the point collocation weighting, $w_i^k = \delta(\vec{r} - \vec{r}_i^k)$, where \vec{r}_i^k is the i th collocation point on surface k . With this choice, \mathbf{A}^k is simplified to an identity matrix, $\mathbf{B}_i^k = \phi_\infty(\vec{r}_i^k)$, and

$$\mathbf{D}_{ij}^{kl} = D^{kl}[\psi_j^l](\vec{r}_i^k) \quad (16)$$

$$\mathbf{G}_{ij}^{kl} = G^{kl}[\psi_j^l](\vec{r}_i^k). \quad (17)$$

In the constant collocation, \mathbf{D}_{ij}^{kl} is geometrically the solid angle spanned by triangle j of surface l at centroid of triangle i of surface k . In the linear collocation, \mathbf{D}_{ij}^{kl} equals a linearly weighted solid angle spanned at node i of surface k by triangles that contain node j of surface l (see formulas in [25]).

2) *Galerkin*: In the Galerkin weighting, w_i^k equals ψ_i^k . Inserting this to (12–15) and applying constant basis functions leads to

$$\mathbf{A}_{ii}^k = A_i^k \quad (18)$$

$$\mathbf{B}_i^k = \int_{T_i^k} \phi_\infty dS \quad (19)$$

$$\mathbf{D}_{ij}^{kl} = \int_{T_i^k} D^{kl}[\psi_j^l] dS \quad (20)$$

$$\mathbf{G}_{ij}^{kl} = \int_{T_i^k} G^{kl}[\psi_j^l] dS, \quad (21)$$

where T_i labels the i th triangle, A_i is the area of triangle i , and \mathbf{A} is a diagonal matrix. With linear basis functions, the

equations are

$$\mathbf{A}_{ij}^k = \int_{N_i^k} \psi_i^k \psi_j^k dS \quad (22)$$

$$\mathbf{B}_i^k = \int_{N_i^k} \psi_i^k \phi_\infty dS \quad (23)$$

$$\mathbf{D}_{ij}^{kl} = \int_{N_i^k} \psi_i^k D^{kl}[\psi_j^l] dS \quad (24)$$

$$\mathbf{G}_{ij}^{kl} = \int_{N_i^k} \psi_i^k G^{kl}[\psi_j^l] dS, \quad (25)$$

where N_i labels the neighborhood of node i : all triangles, which contain the node i .

3) *Computation of Element Integrals*: In case of the point collocation methods, all element integrations were calculated analytically. The double-layer integrals (16) were computed with the Helsinki BEM library [25], which performs the integrations as described in [26], [27]. Single-layer integrations (17) were computed with formulas derived by Graglia: for the constant basis, Eq. (19) of [28], and for the linear basis, Eq. (24) of [28] were used.

In the Galerkin methods, the inner (operator) integrals were calculated as in the collocation methods. The outer integrals, including the integrals in \mathbf{A}_{ij}^k and \mathbf{B}_i^k , were evaluated numerically with the Gaussian quadrature. After testing 7- and 12-point quadratures, the 7-point formula was chosen; the use of the 12-point formula did not have significant effect on results.

D. Transfer Matrices

After discretization and integration, transfer matrices are built. From (9) we get

$$\left(\frac{1}{2} \mathbf{A}^B + \mathbf{D}^{BB} \right)^\dagger \mathbf{B} = \Phi^B, \quad (26)$$

where \dagger labels the inversion of a deflated [29] matrix. In the deflation procedure, the zero potential is, in this study, set equal to the integral of the potential over the body surface.

The forward transfer matrix for the epicardial potential is formed from (10) and (11) by eliminating the Γ -term and then solving for Φ , leading to

$$\Phi^B = \mathbf{L} \Phi^H, \quad (27)$$

$$\mathbf{L} = \left[\left(\frac{1}{2} \mathbf{A}^B + \mathbf{D}^{BB} \right) - \mathbf{G}^{BH} (\mathbf{G}^{HH})^{-1} \mathbf{D}^{HB} \right]^{-1} \cdot \left[\mathbf{D}^{BH} + \mathbf{G}^{BH} (\mathbf{G}^{HH})^{-1} \left(\frac{1}{2} \mathbf{A}^H - \mathbf{D}^{HH} \right) \right]. \quad (28)$$

Each row of the forward transfer matrix \mathbf{L} corresponds to one collocation point on the body surface. The transfer matrix for a subset of the body surface points can thus be formed by choosing only those rows of the full transfer matrix \mathbf{L} , which correspond to the points of interest. In the inverse epicardial potential problem, measurement data is available in electrode positions only. Then it is feasible to build a transfer matrix \mathbf{L}_e , which yields the body surface potential in the electrode positions. If the electrode positions do not match with the collocation points, the electrode-specific transfer matrix can be constructed using the linear basis functions for interpolation of

the potential from the nearest nodes to the electrode positions (not used in this study).

When the body surface potential Φ^B is known, the epicardial potential can be estimated, e.g., by multiplying Φ^B with the inverse of the transfer matrix \mathbf{L} . This inverse potential problem is ill-posed, and \mathbf{L} needs to be regularized before it can be inverted. In this study, the Tikhonov zeroth and second order regularizations (see [6]) were used. In the Tikhonov 2 regularization, the Laplacian matrix on the epicardial surface was built according Eq. (5) in [30]. The regularization parameter λ was optimized so that the relative error of the reconstructed epicardial potential was minimized. Our solutions can thus be called “best-possible Tikhonov solutions” as in [6].

E. Error Measures

The error evaluation was done with the relative error (RE) estimate. The relative error was computed both in the collocation points (cp) and as integral over the surface (int):

$$\text{RE}_{\text{cp}} = \frac{\sqrt{\sum_i [\phi_r(\vec{r}_i) - \phi_t(\vec{r}_i)]^2}}{\sqrt{\sum_i [\phi_r(\vec{r}_i)]^2}} \quad (29)$$

$$\text{RE}_{\text{int}} = \frac{\sqrt{\int (\phi_r - \phi_t)^2 dS}}{\sqrt{\int \phi_r^2 dS}}, \quad (30)$$

where the subscript “r” refers to reference result, and “t” correspondingly to the test result. The integration of RE_{int} was performed numerically with the 7-point Gaussian quadrature. RE_{cp} corresponds to the minimization criterium of the collocation methods, and RE_{int} to the criterium of the Galerkin methods.

In initial analysis, we also used the correlation coefficient (Eq. 35 in [25]). The correlation coefficient showed less difference between the methods than the RE did; this means that differences between the methods are more of the amplitude than of the morphological nature. We did all further analysis with the RE measure.

F. Plots and Statistics

The results of the computations are presented graphically, plotting the median of the relative error as function of source depth. Before taking the median, the results from radial and tangential sources are pooled together. Median instead of mean was chosen, because the error distributions are skewed, partially due to the absolute-value nature of the errors. Statistical significance of the difference of medians was evaluated with the Wilcoxon signed rank test, a non-parametric equivalent to the paired t-test. Briefly, all results pinpointed in the text of the following sections were statistically significant; for results with sources at relative depth ≤ 0.7 and some results with superficial sources (relative depth ≥ 0.8), $p < 0.001$, and for the other mentioned results with superficial sources, $p < 0.05$.

In each plot, there is one curve for each computational method. For the constant basis methods, the data points are marked with open circles, while the data points of the linear methods are marked with black crosses. The line connecting the data points is in case of the collocation methods drawn

solid, and in case of the Galerkin methods dotted. The variation of the error of each method between different sources is visualized with a shaded region around the error curve. The borders of this region are the 16th and 84th percentiles of the dataset, which form a non-parametric equivalent to one standard deviation. The variation regions are plotted with transparent gray: the more regions overlap, the darker the gray.

In Section IV-C3, the results with added modeling error are described. In addition to the basic error plot described in the previous paragraph, these plots contain information for facilitating the comparison to the results in optimal conditions. The median change of the relative error due to the modeling error is plotted as described in the previous paragraph, but without the variation regions. In addition, the variation of the error between different methods is plotted as a bar graph. The height of a bar is equal to the median of the difference between maximum and minimum error for each source in optimal conditions.

G. Outline of Computations

The first step in our evaluation of different basis and weighting functions was to validate the methods and compare them to analytical solutions. The collocation methods were already validated in [25]; here we performed similar, but extended analysis. The second step was to evaluate the performance of different basis and weighting scenarios in the forward calculation of the epicardial potential in a thorax-shaped geometry. In connection to that, the error resulting from the discretization of the epicardial potential was also assessed. The third step was to compare the epicardial inverse solutions produced with different element basis and weighting scenarios. In all computations, care was taken to keep the analysis unbiased.

III. ANALYTICAL VALIDATION

The analytical validation was carried out in a spherical, homogeneous volume conductor with a current dipole source. The analytical solutions were calculated as described by Yao [31]. The surface of the sphere was tessellated into 642 nodes and 1280 triangles. The test sources were placed at 9 equidistant depths between $[0.1R, 0.9R]$, where R is the radius of the sphere. The mean triangle side length was $0.15R$. For each depth, 100 random positions were generated, and for each position, the electric potential generated by a radial and a tangential unit current dipole was calculated.

In similar analysis published earlier [19], [24], the radius of the sphere in the analytical calculations has been scaled in order to match the field calculation points better with the true spherical surface. Ferguson and Stroink [24] experimented with various scalings, while Tissari and Rahola [19] matched the radius of the reference sphere with the mean distance of the quadrature points from the origin. In this work, both non-scaled and scaled spheres were used. In the non-scaled sphere, the nodes of the mesh lie on the surface of the sphere; the faces of the triangles thus lie inside the true spherical surface. In the scaled sphere, the radius of the reference sphere was

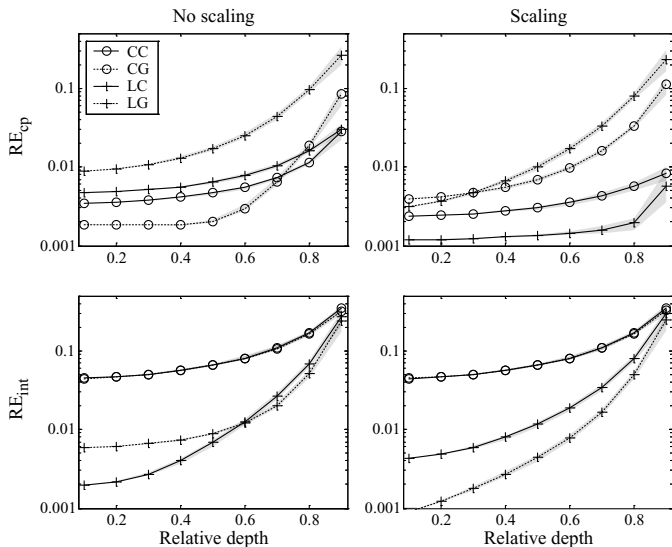


Fig. 1. Median relative error of the electric potential on the surface of a spherical volume conductor with different source depths. For further explanation, see Section II-F.

set equal to the mean distance from the origin to the surface of the triangulated sphere.

Results of these calculations are presented in Fig. 1. In the most simple case, shown on the upper left subplot, no scaling was used and the error was evaluated in the collocation points. In this setup, methods with constant basis performed better than the methods with linear basis. In case of deep and semi-deep sources, the constant Galerkin (CG) method produced the smallest error. For superficial sources, the constant collocation (CC) performed best. At all source depths, the linear Galerkin (LG) method produced the largest error. When scaling was used and error was evaluated in the collocation points (the upper right subplot), the linear collocation method (LC) outperformed other methods. The LG method had again the largest error, except in case of deep sources.

Next, the relative error was evaluated over the whole surface (RE_{int}). The results are shown in the subplots at the bottom row of Fig. 1. Now the linear basis clearly outperformed the constant basis. Results obtained with the CC and CG methods were practically identical. When the reference sphere was not scaled, the LC method had overall the best performance, while the LG method was slightly better with superficial sources. With the scaled sphere, the LG method was superior to the other methods at all source depths.

IV. THORAX-SHAPED GEOMETRY

A. Computational Setup

The forward and inverse computations of epicardial potential were performed in the Dalhousie thorax model [6]. The Dalhousie thorax surface consists of 352 nodes (700 triangles) and the epicardial surface of 202 nodes (400 triangles). The epicardial surface is cut at the level of the valves; it surrounds thus only the ventricles.

Also in computations with the Dalhousie model, single current dipoles were used as sources. The dipoles were placed

at nine equidistant depths inside the epicardial surface. At each depth, 50 randomly positioned dipoles with radial and tangential orientations were created. The same set of sources was used in all calculations in the Dalhousie model.

First, the potential generated by the test dipole on the surface of the thorax was calculated with (9). Then, the potential inside the thorax was calculated with (6). The D^B operator was discretized according to (16). The potential was calculated in 2800 quadrature points over the epicardial surface (from now on called “the accurate epicardial potential”) and also in the collocation points. This approach produces a point collocation solution; using it in connection with the Galerkin method would thus favor the collocation methods. In case of the Galerkin methods, (6) was discretized fully on both epicardial and body surfaces with methods presented in Section II-C2.

The surface and epicardial potentials obtained as described here served as input and reference data in following computations. Both the reference and the test solution were computed with the same set of basis and weight functions, unless stated otherwise.

B. Discretization and Forward Calculation of the Epicardial Potential

The error caused by the discretization of the epicardial potential was assessed by computing the epicardial potential in the collocation points, interpolating it over the surface with the basis functions used in the computation, and then comparing the interpolated potential to the accurate epicardial potential. Median relative errors for each method as function of source depth are displayed in the left subplot of Fig. 2. Methods with linear basis outperformed the constant basis methods, except in case of the LC method and sources very near the epicardial surface. The LG method had the smallest errors at all source depths. Constant methods had almost identical performances in case of deep sources. With superficial sources, the CG method was slightly more accurate than the CC method.

Next, the error due to the use of forward transfer matrix \mathbf{L} (28) with the discretized epicardial potential was studied. The reconstructed body surface potential was calculated with the \mathbf{L} matrix from the discretized epicardial potential, and the result was compared to the original body surface potential that was calculated directly from the source with (9). The error was evaluated in the collocation points only, because in the BEM the potential on a boundary surface outside the collocation points is obtained via interpolation; the use of RE_{int} would thus not lead to a more accurate error estimate over the body surface. The results are displayed in the right subplot of Fig. 2. Again, the LG method had the best performance. Methods using constant potential produced similar errors for deep sources, but in case of sources near the epicardial surface, the CG method performed better than the CC method. For all source depths, the LC method produced the largest error.

C. Inverse Calculation of the Epicardial Potential

1) *Computational Setup*: In the inverse computation of the epicardial potential, we used the Helsinki body surface potential mapping layout containing 120 thoracic electrodes [32].

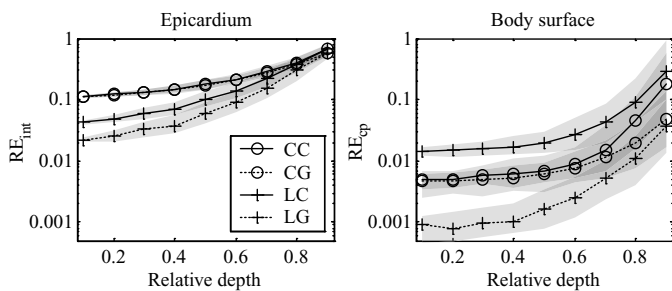


Fig. 2. Errors due to the discretization and forward computation of the epicardial potential for dipolar sources at different depths; on the left subplot is the median integral error on the epicardium, and on the right one the median point-wise error on the body surface. For further explanation, see Section II-F.

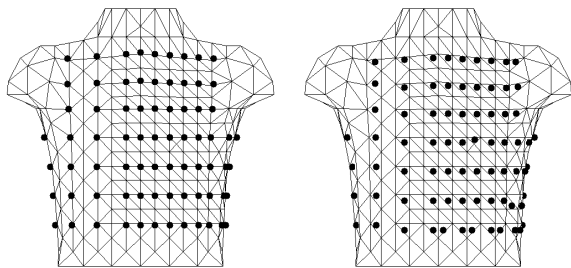


Fig. 3. The Dalhousie thorax model and anterior electrode layouts for linear (on left) and constant basis (on right)

The electrode positions in the Helsinki layout have matching nodes in the Dalhousie thorax model. For calculations with collocation points in the centroids of the mesh triangles, the layout was shifted so that each electrode was placed in a triangle centroid while retaining the geometry of the whole layout. This was done in order to make direct calculations with the L_e matrix possible also with the constant basis functions. Anterior parts of the electrode layouts are visualized in Fig. 3.

The inverse computation of the epicardial potential has commonly been done with a transfer matrix equivalent to our L . The use of the inverse transfer matrix built from the L matrix requires knowledge of the potential on the whole body surface. In practice, the potential is known only in electrode positions. The full body surface potential is in such a case obtained via interpolation. In this study, this interpolation was done by minimizing the surface Laplacian over the body surface as described in [33], refined with a more advanced formulation for the Laplacian (Eq. 5 in [30]).

For each test source, the inverse computation was performed with both Tikhonov 0 and Tikhonov 2 regularizations. Four different scenarios regarding the electrode setup and interpolation were used:

- 1) **Electrodes:** The inverse solution was done with the L_e matrix using the body surface potential data calculated in the electrode points. These results are presented in the left side subplots of Figures 4–6.
- 2) **Interpolation:** The inverse solution was done with the full L matrix. The body surface data were calculated in the electrode points, from which they were interpolated to all collocation points. Results are presented in the

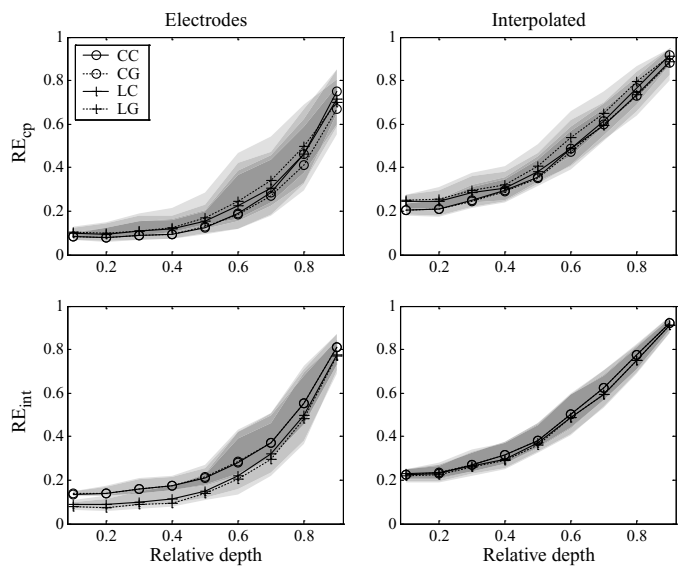


Fig. 4. Median RE_{ep} and RE_{int} in the inverse calculation of the epicardial potential with Tikhonov 2 regularization. For further explanation, see Section II-F.

right side subplots.

- 3) **Collocation points:** The inverse solution was done with the full L matrix and body surface data calculated in all collocation points
- 4) **Cross interpolation:** The inverse solution was done with the full L matrix. For constant methods, the body surface data were calculated with linear basis in the nodal electrode points and interpolated from these nodes to all triangle centroids. For linear methods, the calculations were done with constant basis in the centroid electrode points, and the body surface data were then interpolated to all nodes.

The results of scenario 3 were similar to those of scenario 1, with slightly smaller overall error level. Because there are no electrode setups, which would cover the whole thorax evenly, the scenario 3 has no practical relevance. The results of scenario 3 are hence not presented in this paper. Results of scenario 4 are also left out, because they were practically identical to those of scenario 2.

The median relative error of the body surface potentials due to the interpolation in scenario 2 was between 5.5 and 8.5 percents for deep and superficial sources, respectively. In visual comparison, the interpolated potential was typically slightly smoother than the potential obtained with scenario 3.

In all inverse calculations, the Tikhonov 2 regularization clearly outperformed the Tikhonov 0. Similar results were also obtained earlier [6]. The results obtained with the Tikhonov 0 regularization are thus not presented.

- 2) *Inverse Computation in Optimal Modeling Conditions:* In the first analyses, the inverse potential problem was assessed without adding any error to the model: the reference and the test solutions were computed in identical geometries. This situation is referred to as “optimal conditions”. Results are presented in Fig. 4.

When electrode data were used and the error was evaluated

in the collocation points, differences between the collocation and Galerkin weightings and different basis functions were small (top left plot in Fig. 4). The constant methods produced smaller errors than the linear methods at all source depths. For deep sources, the CC and CG methods had very similar performances, while with superficial sources the CG method was better. Also the linear methods had similar performances with deep sources. When the source was brought closer to the surface, the LC method produced slightly smaller error than the LG method.

In case of electrode data and integrated error (bottom left in Fig. 4), the linear methods produced smaller errors than the constant ones at all source depths. In all calculations, the LG method yielded the smallest errors. The differences between errors produced by linear and constant methods were larger than in other scenarios or in any computations done with the RE_{cp} estimate.

When the inverse reconstruction was performed with interpolated data, the error was at all source depths clearly larger than in case of the electrode data. For RE_{int} , the differences between the methods were smaller than in case of electrode data.

3) *Inverse Computation with Added Modeling Errors:* In the following analysis, errors were included in the anatomical model. First, the epicardial surface was moved 5 mm towards the anterior thorax, while keeping the source positions fixed relative to the epicardium. The forward and epicardial reference solutions were calculated in this geometry, and the inverse calculations were performed in the original geometry. Results are displayed in Fig. 5.

In case of electrode data (Fig. 5, the left column), the error behavior was similar to that in the optimal conditions, but with larger overall error level. For RE_{cp} , the error increase was larger than the error variation between different methods in the optimal conditions, except in case of superficial sources. For RE_{int} , there was no performance difference between the LC and LG methods or the CC and CG methods. The linear methods suffered more from the modeling error than the constant methods did. The overall error increase was of the same order with the variation of RE_{int} in the optimal conditions.

In case of interpolated data (Fig. 5, the right column) and deep sources, the error increased slightly, but for superficial sources it even decreased. With interpolated data, all methods produced practically the same RE_{int} . The error increase was in general smaller than the error variation between different methods. The error level was higher than in case of electrode data.

In the second error scenario, the body surface potential and the reference epicardial potential were calculated with poorly conducting lungs included in the model (lungs-thorax conductivity ratio 1:4). The inverse transfer was computed with the transfer matrix of the homogeneous model. Results are displayed in Fig. 6.

When using only the electrode data, the increase of the error was larger than in the earlier analysis with the position error. With RE_{int} , the LG method suffered most and the CG method least from the added modeling error. The error increase was

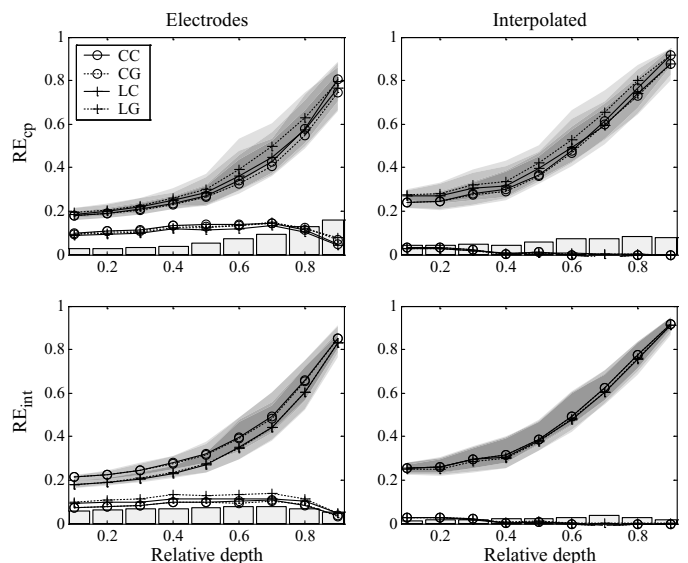


Fig. 5. Relative error in the inverse calculation of the epicardial potential with Tikhonov 2 regularization, when there is a 5 mm error in the position of the epicardial surface. Upper sets of curves in each subplot: median RE with the shifted model; Lower sets of curves: median increase of errors compared to the optimal conditions; Bars: Variation of error between different methods in the optimal conditions. For further explanation, see Section II-F.

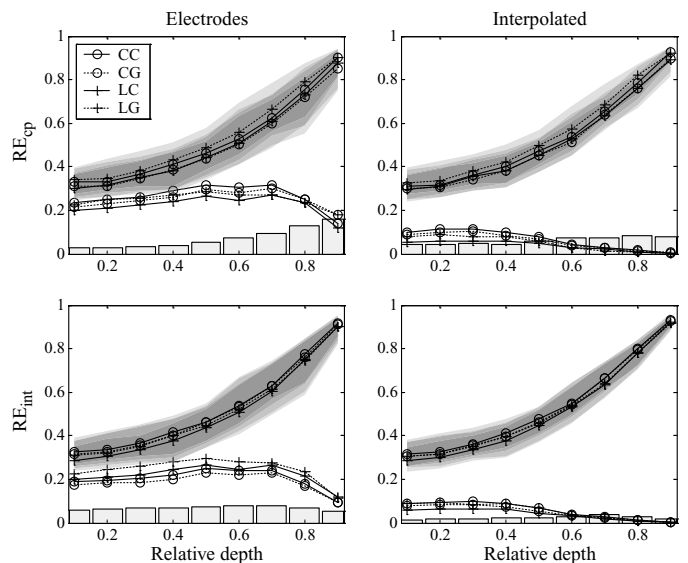


Fig. 6. Relative error in the inverse calculation of the epicardial potential with Tikhonov 2 regularization, when the lungs are included in the calculation of the reference potential but not in the inverse solution. Upper sets of curves in each subplot: median RE with the erroneous model; Lower sets of curves: median increase of errors compared to the optimal conditions; Bars: Variation of error between different methods in the optimal conditions. For further explanation, see Section II-F.

with both error estimates larger than the variation of the error between different methods in the optimal conditions.

With the interpolated data, the errors increased little or not at all, and RE_{int} even decreased for superficial sources. The error performances of electrode and interpolated data were practically identical.

V. DISCUSSION

A. Formulation of the Equations

The operator notation used in our formulation of the integral equations is not commonly used in biomedical engineering. The notation is compact, and the shape of the equations does not change in the discretization process. The use of operators also facilitates the programming of element solvers. For example, consider (7) and (8): These equations are commonly presented as

$$P^{BB}\phi^B + P^{BH}\phi^H + G^{BH}\Gamma^H = 0 \quad (31)$$

$$P^{HB}\phi^B + P^{HH}\phi^H + G^{HH}\Gamma^H = 0, \quad (32)$$

where G , P^{HB} , and P^{BH} correspond to our G , D^{HB} and D^{BH} , respectively. Operations P^{HH} and P^{BB} , however, are equivalent to our $D^{HH} - 1/2$ and $D^{BB} + 1/2$. Because of this inconsistent formulation, the label P loses its geometrical meaning. In our formulation, all geometrical relations are readily available and labels are uniquely defined.

B. Element Integrals

Element integrations of the G matrix have in earlier works been carried out numerically. When the field point is in the integration domain, the integral of (2) contains a weak singularity. Methods for approximating the singular integral have been successfully used [5]–[7], but the error caused by these approximations has been a subject of discussion: Recently, Wang and Rudy applied the method of fundamental solutions (MFS) to the epicardial potential problem [34], discussing the singular integrals as an important problem of the BEM. Horáček and Clements [6] discussed that the numerical quadrature used in the singularity extraction may decrease the performance of their LC computations. However, the integral of (17) can, at least in case of constant and linear basis functions, be calculated analytically as described by Graglia [28]. The use of analytical integration simplifies the programming and computations and removes one factor of uncertainty from the computations. However, the use of accurate integrals does not necessarily lead to better results, as Mosher et al. discussed in [20].

C. Analytical Validation

The results presented in Section III show that no method is optimal in all our test scenarios and for all source depths. The only clear result is that when the error is evaluated over the whole surface, the linear methods outperform the constant ones. This is easy to accept: in constant potential methods, the potential is assumed constant over each whole triangle, while in the linear methods, the potential is interpolated linearly between the nodal potential values, thus being likely to follow the continuous reference data better than the constant interpolation. The same reasoning applies to further results as well.

When the error was analyzed in the collocation points (RE_{cp}) and no scaling was used, the CC method performed better at all source depths than the LC method, whereas in the scaled sphere the situation was opposite. This result was

unexpected: in the non-scaled sphere, the nodes are on the same surface with the sphere of the reference solution, and in the scaled sphere the centroid points are closer to the reference surface than the nodes are. One might hereby hypothesize that the LC method would suffer and the CC method benefit from the scaling, but results showed the opposite.

When the relative error was integrated over the surface (RE_{int}), the LC method performed better than the LG method with deep and semi-deep sources, when no scaling was used. This is surprising, as the error evaluation scenario favors the LG method. Only when the scaling was used in connection with the RE_{int} measure, the LG method outperformed the other methods. The results of Tissari and Rahola [19] favored the LG method. Their analysis was done using only one scenario with a scaled sphere and error evaluation in a dense point set (13 points in a triangle) — a scenario very similar to our scaled sphere and RE_{int} measure.

D. Discretization and Forward Calculation of the Epicardial Potential

In order to get good solutions to the inverse problem, an accurate forward transfer is important, regardless of the specific inverse techniques: errors due to the forward transfer can not be corrected in later phases of the analysis. The results in Section IV-B show that the smallest error in the forward computation is obtained with the LG method. The largest error resulted from the LC method. The CG method was better than the CC method, especially with superficial sources. One reason for the large errors with the LC method is the so-called auto-solid angle problem and how it is dealt with [24]; we used the method suggested by de Munck [24], [27]. With the CC, CG, and LG methods the auto-solid angle causes no problem as the calculations are performed in the smooth triangles instead of nodes.

Horáček and Clements performed similar analysis with the same volume conductor model using a single deep-lying dipole source and constant and linear collocation methods [6]. Comparing the results, the errors in the forward transfer with the CC method were of the same order, but our values were slightly smaller: Horáček and Clements reported a relative error of 0.92%, while our calculations with the CC method and deep sources produced median error of 0.51%, ranging between 0.19% and 0.88%. The difference may be due to our use of analytical integration in G operations, but it can result from any difference in the numerical treatments, too.

In case of linear basis functions, Horáček and Clements [6] reported the relative error of 5.3%, while the median error in our calculations was 1.5%, ranging between 0.98 and 1.8 percents. It is, however, not apparent, whether the reference solution used by Horáček and Clements was calculated directly or interpolated from the constant potential solution; if interpolation was used, it explains the worse results. The numerical integrations used by Horáček and Clements in both P and G operations are likely to form part of the error as well. To provide comparison to the numbers presented here, our LG method with deep sources yielded a median error of 0.09%, with values ranging between 0.03 and 0.16 percents.

The error resulting from the discretization of the epicardial potential has, to the authors' knowledge, not been assessed before. The discretization error curves serve as good reference, when analyzing the error sources in modeling or optimizing the meshes. The discretization error is also the theoretical minimum of the integrated error (RE_{int}) in the inverse transfer. Results from the analysis of the discretization error show that the linear methods outperform the constant ones, and the LG method produces the smallest errors at all source depths. The success of the LG method was expected, as the Galerkin approach aims at minimizing this kind of error. The CG method, despite the Galerkin weighting, did not perform better than the CC method. Overall, the discretization error is relatively large for the constant methods: it exceeds 10% for all source depths. With superficial sources, all methods produce over 20% discretization errors. This is not surprising, as sources at relative depths 0.8 and 0.9 are on average only 0.57, and 0.29 triangle sidelengths away from the nearest surface point. In practice, an epicardial mesh like the one used here is too coarse for accurate characterization of small-scale cardiac electrical events. With relation to the forward transfer errors, the discretization error comes across as large. These numbers can, however, not be compared, because the forward transfer error was assessed in the collocation points only.

E. Inverse Calculation of Epicardial Potential

The errors present in the inverse calculation of the epicardial potential were assessed both in optimal modeling conditions and in two scenarios with added modeling errors. The results of these calculations are only valid in case of Tikhonov 0 and Tikhonov 2 regularizations; generalizations to other inverse computation scenarios can not be made.

In all calculations, the Tikhonov 2 regularization outperformed the Tikhonov 0. When the error was evaluated in the collocation points (RE_{cp}), differences between the basis functions and weighting methods were small. In general, either the CC or the CG method produced the smallest error.

Comparison of the relative errors to those obtained by Horáček and Clements [6] resembles the forward transfer comparison done in Section V-D: The errors with the CC method are of the same order, our computations producing slightly smaller values. In our computations, the LC method performed better than in those of Horáček and Clements, but worse than the CC method. Horáček and Clements discussed that the poorer performance of the LC method is due to the numerical quadratures. Our study confirms their results and shows that some accuracy difference remains also with analytically integrated elements.

When the error was evaluated over the whole epicardial surface (RE_{int}), the difference between the methods was larger than in case of RE_{cp} . The linear methods produced smaller errors than the constant methods did in all calculations. In the optimal conditions, the LG method produced the smallest errors. In computations with displaced epicardium, the difference between the LG and LC methods got smaller, and in the scenario with the omitted lungs there was no visible difference.

The modeling error resulting from a 5 mm displacement of the epicardium added up to ten percentage units to the

relative error, when the computations were performed with the electrode data. The increase of the error was of the same order as the error variation between the methods. When RE_{cp} was used, all methods suffered practically as much from the displacement. In case of RE_{int} , the linear methods suffered more from the modeling error than the constant methods did.

When the lungs were included in the reference but not in the test solution, the error grew on average by 20 percentage units. The increase was considerably larger than the variation of the error between the methods. Hereby we can say that the choice of the computational method is not important, if large modeling errors such as omission of the lungs are present. The importance of modeling of the lungs has also been demonstrated in a phantom study regarding focal source localization in electro- and magnetocardiography [35]. In most publications regarding epicardial potential computation, including recent works presenting novel computational techniques [9], [34], lungs have been omitted.

When interpolated full thorax data were used, differences between the methods were smaller than in case of the electrode data. The errors in the optimal conditions were larger, but modeling errors had smaller effect on results than in case of the electrode data. Overall, the error behavior was less dependent on the modeling and error evaluation conditions than with the electrode data. When the lungs were included in the reference solution but omitted in the inverse calculation, the interpolated data performed, according to visual inspection of the error curves, equivalently with the electrode data. In numerical comparison, the electrode data yielded smaller errors also in this case. In practice, interpolation would likely produce larger errors than in this simulation study due to the modeling errors involved at the extremities of the model. Hence we see no reason for interpolating the data from the electrode points over the whole thorax.

When comparing the performance of the constant and linear methods, it is important to keep in mind that the electrode layouts were optimized for each method. For example, if the segmentation method places nodes at electrode positions, linear methods are likely to perform better than the constant methods; interpolation from the nodes containing the electrodes to the centroids (the cross interpolation scenario in Section IV-C) would likely lead to errors equivalent to those produced with the interpolated data.

VI. CONCLUSIONS

In this work, the use of constant and linear collocation and Galerkin methods in bioelectrical forward and inverse problem were studied. The focus was on the epicardial potential problem.

In analytical validation, no combination of basis and weighting functions was preferable to others in all situations. In discretization and forward computation of the epicardial potential, the linear Galerkin (LG) method performed best.

The electrode-specific transfer matrix L_e is preferable over the full transfer matrix L and the Tikhonov 2 regularization over the Tikhonov 0. In optimal modeling conditions, the best combination of basis and weight functions depends on

electrode positions and chosen error evaluation technique. When large modeling errors are present, the choice of the basis and weighting functions is not significant.

REFERENCES

- [1] H. Oster, B. Taccardi, R. Lux, P. Ershler, and Y. Rudy, "Noninvasive electrocardiographic imaging: Reconstruction of epicardial potentials, electrograms, and isochrones and localization of single and multiple electrocardiac events," *Circulation*, vol. 96, pp. 1012–1024, 1997.
- [2] C. Ramanathan, R. Ghanem, P. Jia, K. Ryu, and Y. Rudy, "Noninvasive electrocardiographic imaging for cardiac electrophysiology and arrhythmia," *Nature Med.*, vol. 10, no. 4, pp. 422–428, 2004.
- [3] R. Ghanem, P. Jia, C. Ramanathan, K. Ruy, A. Markowitz, and Y. Rudy, "Noninvasive electrocardiographic imaging (ECGI): Comparison to intraoperative mapping in patients," *Heart Rhythm*, vol. 2, no. 2, pp. 339–354, 2005.
- [4] C. Brebbia and J. Dominguez, *Boundary Elements: an Introductory Course*. New York: McGraw-Hill, 1989.
- [5] R. Barr, M. Ramsey, and M. Spach, "Relating epicardial to body surface potential distributions by means of transfer coefficients based on geometry measurements," *IEEE Trans. Biomed. Eng.*, vol. BME-24, pp. 1–11, Jan. 1977.
- [6] B. Horáček and J. Clements, "The inverse problem of electrocardiography: A solution in terms of single- and double-layer sources on the epicardial surface," *Math. Biosci.*, vol. 144, pp. 119–154, 1997.
- [7] M. Stenroos, H. Hänninen, M. Lindholm, I. Tierala, and T. Katila, "Lead field formulation for epicardial potential in electrocardiographic localization of acute myocardial ischemia," in *Proc. IFMBE, 3rd European Medical & Biological Engineering Conference, Prague*, vol. 11, 2005, pp. 2265–1 – 2265–5.
- [8] R. MacLeod, M. Gardner, R. Miller, and B. Horáček, "Application of an electrocardiographic inverse solution to localize ischemia during coronary angioplasty," *J. Cardiovasc. Electrophysiol.*, vol. 6, no. 1, pp. 2–18, 1995.
- [9] S. Ghosh and Y. Rudy, "Accuracy of quadratic versus linear interpolation in noninvasive electrocardiographic imaging (ECGI)," *Ann. Biomed. Eng.*, vol. 33, no. 9, pp. 1187–1201, 2005.
- [10] G. Fischer, B. Tilg, P. Wach, R. Modre, U. Leder, and H. Nowak, "Application of high-order boundary elements to the electrocardiographic inverse problem," *Comput. Methods Programs Biomed.*, vol. 58, pp. 119–131, 1999.
- [11] G. Fischer, B. Tilg, R. Modre, F. Hanser, B. Messnarz, and P. Wach, "A Galerkin boundary element formulation for cardiac activation time imaging," *Int. J. Bioelectromag.*, vol. 4, no. 2, pp. 83–84, 2001.
- [12] R. Modre, B. Tilg, G. Fischer, F. Hanser, B. Messnarz, M. Seger, F. Hintringer, and F. Roithinger, "Ventricular surface activation time imaging from electrocardiogram mapping data," *Med. Biol. Eng. Comput.*, vol. 42, pp. 146–150, 2004.
- [13] M. Seger, G. Fischer, R. Modre, B. Messnarz, F. Hanser, and B. Tilg, "Lead field computation for the electrocardiographic inverse problem — finite elements versus boundary elements," *Comput. Methods Programs Biomed.*, vol. 77, pp. 241–252, 2005.
- [14] G. Huiskamp and A. van Oosterom, "The depolarization sequence of the human heart surface computed from measured body surface potentials," *IEEE Trans. Biomed. Eng.*, vol. 35, pp. 1047–1058, Dec. 1988.
- [15] R. MacLeod and D. Brooks, "Recent progress in inverse problems in electrocardiology," *IEEE Eng. Med. Biol.*, vol. 17, pp. 73–83, Jan./Feb. 1998.
- [16] P. Colli-Franzone, L. Guerri, S. Tentoni, C. Viganotti, S. Baruffi, S. Spaggiari, and B. Taccardi, "A mathematical procedure for solving the inverse potential problem of electrocardiography. Analysis of the time-space accuracy from in vitro experimental data," *Math. Biosci.*, no. 1–2, pp. 353–396.
- [17] A. V. Shahidi and P. Savard, "Forward and inverse problems of electrocardiography: Modeling and recovery of epicardial potentials in humans," *IEEE Trans. Biomed. Eng.*, vol. 41, pp. 249–256, Mar. 1994.
- [18] A. Pullan, "A high-order coupled finite element/boundary element torso model," *IEEE Trans. Biomed. Eng.*, vol. 43, pp. 292–298, Mar. 1996.
- [19] S. Tissari and J. Rahola, "Error analysis of a Galerkin method to solve the forward problem in MEG using the boundary element method," *Comput. Methods Programs Biomed.*, vol. 72, pp. 209–222, 2003.
- [20] J. Mosher, R. Leahy, and P. Lewis, "EEG and MEG: Forward solutions for inverse methods," *IEEE Trans. Biomed. Eng.*, vol. 46, pp. 245–259, Mar. 1999.
- [21] C. Ramanathan and Y. Rudy, "Electrocardiographic imaging: II. Effect of torso inhomogeneities on noninvasive reconstruction of epicardial potentials, electrograms, and isochrones," *J. Cardiovasc. Electrophysiol.*, vol. 12, pp. 241–252, Feb. 2001.
- [22] R. Plonsey and D. Heppner, "Considerations of quasistationarity in electrophysiological systems," *Bull. Math. Biophys.*, vol. 29, pp. 657–664, 1967.
- [23] D. Geselowitz, "On bioelectric potentials in an inhomogeneous volume conductor," *Biophys. J.*, vol. 7, pp. 1–11, 1967.
- [24] A. Ferguson and G. Stroink, "Factors affecting the accuracy of the boundary element method in the forward problem I: Calculating the surface potentials," *IEEE Trans. Biomed. Eng.*, vol. 44, pp. 1139–1155, Nov. 1997.
- [25] M. Stenroos, V. Mäntynen, and J. Nenonen, "A Matlab library for solving quasi-static volume conduction problems using the boundary element method," *Comput. Methods Programs Biomed.*, vol. 88, pp. 256–263, 2007.
- [26] A. van Oosterom and J. Strackee, "The solid angle of a plane triangle," *IEEE Trans. Biomed. Eng.*, vol. BME-30, pp. 125–126, Feb. 1983.
- [27] J. de Munck, "A linear discretization of the volume conductor boundary integral equation using analytically integrated elements," *IEEE Trans. Biomed. Eng.*, vol. 39, pp. 986–989, Sep. 1992.
- [28] R. Graglia, "On the numerical integration of the linear shape functions times the 3-D Green's function or its gradient on a plane triangle," *IEEE Trans. Antennas Propag.*, vol. 41, pp. 1448–1455, Oct. 1993.
- [29] G. Fischer, B. Tilg, F. Hanser, B. Messnarz, and P. Wach, "On modeling the Wilson terminal in the boundary and finite element method," *IEEE Trans. Biomed. Eng.*, vol. 49, pp. 217–224, Mar. 2002.
- [30] G. Huiskamp, "Difference formulas for the surface Laplacian on a triangulated surface," *J. Comput. Phys.*, vol. 95, no. 2, 1991.
- [31] D. Yao, "Electric potential produced by a dipole in a homogeneous conducting sphere," *IEEE Trans. Biomed. Eng.*, vol. 47, pp. 964–966, Jul. 2000.
- [32] K. Simelius, I. Tierala, T. Jokiniemi, J. Nenonen, L. Toivonen, and T. Katila, "A body surface potential mapping system in clinical use," *Med. Biol. Eng. Comput.*, no. S1, Part 2, pp. 107–108.
- [33] T. Oostendorp, A. van Oosterom, and G. Huiskamp, "Interpolation on a triangulated 3D surface," *J. Comput. Phys.*, no. 2, pp. 331–343.
- [34] Y. Wang and Y. Rudy, "Application of the method of fundamental solutions to potential-based inverse electrocardiography," *Ann. Biomed. Eng.*, vol. 34, no. 8, pp. 1272–1288, 2006.
- [35] U. Tenner, J. Hauelsen, H. Nowak, U. Leder, and H. Brauer, "Source localization in an inhomogeneous physical thorax phantom," *Phys. Med. Biol.*, vol. 44, pp. 1969–1981, 1999.



Matti Stenroos received the M.Sc. and Lic.Sc. degrees in engineering physics and mathematics from the Helsinki University of Technology (TKK) in 2002 and 2005, respectively.

He is currently a researcher and lecturer in the Department of Biomedical Engineering and Computational Science at the Helsinki University of Technology. His research interests include numerical calculation of bioelectric fields, and body surface potential mapping applications.



Jens Hauelsen (M '03) received the M.S. and Ph.D. degrees in electrical engineering from the Technical University Ilmenau, Ilmenau, Germany, in 1992 and 1996, respectively.

From 1996 to 1998, he worked as a Postdoctoral Researcher, and from 1998 to 2005, as the Head of the Biomagnetic Center, Friedrich-Schiller-University, Jena, Germany. Since 2005, he has been the Professor of Biomedical Engineering and the Director of the Institute of Biomedical Engineering and Informatics at the Technical University Ilmenau.

His research interests are in the numerical computation of bioelectric and biomagnetic fields and biological signal analysis.